Concentrated flow erodibility for physically based erosion models: Temporal variability in disturbed and undisturbed rangelands

Osama Z. Al-Hamdan,[1,2] Frederick B. Pierson,[1] Mark A. Nearing,[3] C. Jason Williams,[1] Jeffry J. Stone,[3] Patrick R. Kormos,[4] Jan Boll,[2] and Mark A. Weltz[5]

Received 29 September 2011; revised 23 March 2012; accepted 25 May 2012; published 7 July 2012.

[1] Current physically based overland flow erosion models for rangeland application do not separate disturbed and undisturbed conditions in modeling concentrated flow erosion. In this study, concentrated flow simulations on disturbed and undisturbed rangelands were used to estimate the erodibility and to evaluate the performance of linear and power law equations that describe the relationship between erosion rate and several hydraulic parameters. None of the hydraulic parameters consistently predicted the detachment capacity well for all sites, however, stream power performed better than most of other hydraulic parameters. Using power law functions did not improve the detachment relation with respect to that of the linear function. Concentrated flow erodibility increased significantly when a site was exposed to a disturbance such as fire or tree encroachment into sagebrush steppe. This study showed that burning increases erosion by amplifying the erosive power of overland flow through removing obstacles and by changing the soil properties affecting erodibility itself. However, the magnitude of fire impact varied among sites due to inherent differences in site characteristics and variability in burn severity. In most cases we observed concentrated flow erodibility had a high value at overland flow initiation and then started to decline with time due to reduction of sediment availability. Thus we developed an empirical function to predict erodibility variation within a runoff event as a function of cumulative unit discharge. Empirical equations were also developed to predict erodibility variation with time postdisturbance as a function of readily available vegetation cover and surface soil texture data.

Citation: Al-Hamdan, O. Z., F. B. Pierson, M. A. Nearing, C. J. Williams, J. J. Stone, P. R. Kormos, J. Boll, and M. A. Weltz (2012), Concentrated flow erodibility for physically based erosion models: Temporal variability in disturbed and undisturbed rangelands, *Water Resour. Res.*, *48*, W07504, doi:10.1029/2011WR011464.

1. Introduction

[2] Erosion rates on rangelands tend to be relatively low, but under certain conditions soil loss can be significant. On most undisturbed rangelands, soil loss is minimal and occurs primarily by rain splash and sheet erosion. However, concentrated flow is commonly the dominant mechanism of water erosion following disturbance on steep slopes or where ground cover is sparse [*Pierson et al.*, 2009]. The lack of studies that explain concentrated flow erosion across diverse rangeland ecosystems has resulted in the use of cropland-based equations for rangeland hydrology and erosion modeling [e.g., *Elliot et al.*, 1989; *Nearing et al.*, 1989; *Simanton et al.*, 1991], which may lead to less accurate predictions as rangelands and croplands have different soil and vegetation cover characteristics.

[3] Most physically based erosion models separate the erosion process descriptions into concentrated flow (rill) erosion and splash and sheet (inter-rill) erosion [*Foster*, 1982; *Hairsine and Rose*, 1992; *Flanagan and Nearing*, 1995]. In most cases, splash and sheet erosion is determined by rainfall intensity and runoff rate [*Wei et al.*, 2009]. Concentrated flow erosion is usually determined by flow hydraulic parameters and/or flow transport capacity [*Knapen et al.*, 2007a].

[4] When using a hydraulic parameters approach, such as shear stress, concentrated flow erosion is often considered to be a threshold phenomenon where the soil detachment rate can be related to the exceedance of a hydraulic parameter value with respect to its critical value. The general formula for such a model is

$$D_{cf} = K_{HP}(HP - HP_c)^{\alpha}, \quad (1)$$

where D_{cf} is the concentrated flow soil detachment rate capacity (kg s^{-1} m^{-2}), K_{HP} is the soil erodibility factor based on the hydraulic parameter HP, HP_c is the threshold

[1]USDA, Agricultural Research Service, Northwest Watershed Research Center, Boise, Idaho, USA.
[2]Department of Biological and Agricultural Engineering, University of Idaho, Moscow, Idaho, USA.
[3]USDA, Agricultural Research Service, Southwest Watershed Research Center, Tucson, Arizona, USA.
[4]Department of Geosciences, Boise State University, Boise, Idaho, USA.
[5]USDA, Agricultural Research Service, Exotic and Invasive Weeds Research Unit, Reno, Nevada, USA.

Corresponding author: O. Z. Al-Hamdan, USDA, Agricultural Research Service, Northwest Watershed Research Center, 800 Park Blvd., Plaza IV, Boise, ID 83712-7716, USA. (osama.al-hamdan@ars.usda.gov)

value where D_{cf} is insignificant before HP exceeds it, and α is the power exponent. Several forms of equation (1) have been developed, however, most of these equations were obtained from research conducted on cropland soils in field and laboratory studies [e.g., *Nearing et al.*, 1989; *Franti et al.*, 1999; *Zhu et al.*, 2001; *Giménez and Govers*, 2002; *Zhang et al.*, 2003]. *Zhu et al.* [2001] suggested that power law relationships accurately predict the detachment rate, but linear forms of equation (1) (i.e., assuming $\alpha = 1$) simplify model parameterization. In a study conducted on undisturbed rangeland in Arizona, USA, *Nearing et al.* [1999] found detachment rates from artificial rills were well correlated to a power law form of equation (1) with either shear stress or stream power as the hydraulic parameter.

[5] In the past few years, efforts have been increased to develop physically based overland flow erosion models specifically parameterized for rangelands processes. For instance, *Nearing et al.* [2011] developed the Rangeland Hydrology and Erosion Model (RHEM). The current version of RHEM does not differentiate between disturbed sites (e.g., burned sites) and undisturbed sites in modeling erosion of concentrated flow. The model uses an approach that assumes constant concentrated flow erodibility for each runoff event. However, recent studies on burned rangelands suggested that concentrated flow sediment concentration varies during experiments using a constant flow rate, where it is higher in the early part of a runoff event than in the latter part [*Moffet et al.*, 2007; *Pierson et al.* 2008]. The same trend was also reported for a forest road site [*Foltz et al.*, 2008] and burned forest sites [*Wagenbrenner et al.*, 2010]. The assumption of constant erodibility within an overland flow event might be acceptable for most cases in cropland where the structure of the soil layers is altered by frequent tillage, producing a continuous/ample sediment source from deep layers. In contrast, rangeland soils are often shallow and nonuniform (i.e., variable particle sizes and rock content), yielding an inconsistent supply and type of material available for erosion and therefore a varying erodibility. The inconsistency of supply and type of material available for erosion is more evident in disturbed sites (e.g., burned sites) where significant amount of protected supply becomes suddenly available. Therefore, any estimate of concentrated flow erosion on such sites should take into account the variability of the concentrated flow erodibility during a runoff event.

[6] The main goal of this study was to estimate concentrated flow soil erodibility parameters from disturbed and undisturbed rangeland field data for use in physically based erosion models. To reach the main goal, the specific objectives of this study were to (1) characterize the relationship between concentrated flow detachment capacity and commonly derived hydraulic parameters for different rangeland environmental conditions; (2) develop a model that predicts soil erodibility changes within a runoff event; (3) investigate the effects of varying degrees of disturbance on magnitude and temporal variability in soil erodibility; and (4) develop empirical equations for estimating concentrated flow soil erodibility based on readily measureable ecological sites, soils, and vegetation data.

2. Theory

[7] Several hydraulic parameters have been used for estimating sediment detachment rate. The most common parameters are: flow shear stress (τ_s) (kg s^{-2} m^{-1}) [e.g., *Nearing et al.*, 1989; *Flanagan and Nearing*, 1995], stream power (ω) (kg s^{-3}) [e.g., *Hairsine and Rose*, 1992; *Elliot and Laflen*, 1993; *Nearing et al.*, 1997], unit stream power (Ω) (m s^{-1}) [e.g., *Moore and Burch*, 1986; *Morgan et al.*, 1998], unit length shear force (Γ) (kg s^{-2}) [e.g., *Giménez and Govers*, 2002], and unit discharge (q) (m^2 s^{-1}) [e.g., *Line and Meyer*, 1989]. These parameters are defined in the following equations:

$$\tau_s = \left(\frac{f_s}{f_t}\right)\gamma R_h \sin[\tan^{-1}(S)], \tag{2}$$

$$\omega = \gamma S q, \tag{3}$$

$$\Omega = V \sin[\tan^{-1}(S)], \tag{4}$$

$$\Gamma = \gamma A \sin[\tan^{-1}(S)], \tag{5}$$

$$q = Q/w, \tag{6}$$

where f_s is the hydraulic friction due to the soil grains, f_t is the total Darcy-Weisbach friction factor, S is the average slope of the plot (m m^{-1}), γ is the specific weight of water (kg m^{-2} s^{-2}), R_h is the hydraulic radius (m), V is the flow velocity (m s^{-1}), A is the flow cross section area (m^2), and Q is the flow discharge (m^3 s^{-1}).

[8] Assuming α is equal to one in equation (1) makes the equation linear:

$$D_{cf} = K_{HP}(HP - HP_c). \tag{7}$$

Equation (7) is most generally used for physically based erosion models especially when HP is represented with shear stress [*Knapen et al.*, 2007a]. For instance, the RHEM model uses the equation for estimating the detachment capacity of a rill (D_{cf}) (kg s^{-1} m^{-2}). The detachment capacity is used to calculate the detachment rate (D_r) (kg s^{-1} m^{-2}) in RHEM by this equation:

$$D_r = D_{cf}\left(1 - \frac{G}{T_c}\right), \tag{8}$$

where G is the sediment transport rate (kg s^{-1}) and T_c is the sediment transport capacity (kg s^{-1}).

3. Material and Methods

3.1. Study Sites

[9] The data used in this study were obtained from rangeland field experimental work by the USDA-ARS Northwest Watershed Research Center, Boise, Idaho. The work, conducted from 2000 to 2008, resulted in 393 experimental plots with concentrated flow. The data were collected from rangeland sites located in the states of Idaho, Nevada, Oregon, and Utah, all within the Great Basin Region, United States. These data span a wide range of slope angles (5.6%–65.8%), soil types (silt loam to coarse sandy loam), and vegetative cover (Table 1). The texture of sand, silt,

Table 1. Location, Land Management Treatments, Dominant Plant Community, Soil Type Description, and Slope for Each Rangeland Field Site in This Study

Site	State	Treatment	Plant Community	Soil Type	Slope Percent
Breaks[a]	ID	Burned,[b] Untreated	Mountain Big Sagebrush	Kanlee-Ola course sandy loam	34.7–56.9
Castlehead[c]	ID	Burned,[b] Cut (Short-term impact[d]), Untreated	Western Juniper/Mountain Big Sagebrush	Mulshoe-Squawcreek-Gaib stoney loam	13.1–23.5
Denio[e]	NV	Burned,[b] Untreated	Mountain Big Sagebrush	Ola boulder sandy loam	26.1–65.7
Marking Corral[f]	NV	Burned,[b] Cut (Short-term impact[d]), Untreated	Single Leaf Pinyon-Utah Juniper/ Wyoming Big Sagebrush	Segura-Upatad-Cropper gravelly loam	6.0–21.3
Onaqui[f]	UT	Burned,[b] Tree mastication, Cut (Short-term impact[d]), Untreated	Utah Juniper/Wyoming Big Sagebrush	Borvant gravelly loam	9.0–26.1
Steens[g]	OR	Cut (Long-term impact[h]), Uncut	Western Juniper/Basin Big Sagebrush	Pernty gravelly cobbly silt loam	15.5–21.7
Upper Sheep[i]	ID	Burned,[b] Untreated	Mountain Big Sagebrush	Harlem silt or Harlem silt loam	29.2–39.3
Upper Sheep[i]	ID	Burned,[b] Untreated	Low Sagebrush	Harlem gravelly silt loam	12.4–22.5

[a][*Pierson et al.*, 2009]
[b]Experiments conducted 0, 1, 2, and 3 growing seasons (years) after fire in Breaks and Denio; 1, 2 years after fire in Marking Corral and Onaqui; and 1 year after fire in Castlehead and Upper Sheep.
[c][*McIver et al.*, 2010]
[d]Experiments conducted within 1 year after cutting.
[e][*Pierson et al.*, 2008]
[f][*Pierson et al.*, 2010]
[g][*Pierson et al.*, 2007]
[h]Experiments conducted 10 years after cutting.
[i][*Flerchinger and Cooley*, 2000]

and clay for each site is shown in Table 2. The vegetation community ranges from sagebrush steppe to wooded (pinyon and/or juniper) shrublands. Many of the sites exhibit some degree of disturbance, such as wildfire, prescribed fire, tree encroachment, and tree removal by mastication and/or cutting (Table 1). Numerous rectangular plots (approximately 4 m long by 2 m wide) were selected at each site, encompassing all treatments for the respective site. At wooded-shrubland sites, plots were set either in the shrub-interspace (area between tree canopies) or on a tree coppice (area underneath the tree canopy). Average slope, canopy and ground cover, and microtopography were measured for each plot [see *Pierson et al.*, 2007, 2008, 2009, 2010].

3.2. Measurement and Calculation of Hydraulic Parameters

[10] Overland flow was simulated on each experimental plot for a range of flow rates on near saturated surface soil conditions. Detailed descriptions of overland flow simulations and plot designs are provided by *Pierson et al.* [2007, 2008, 2009, 2010]. Surface soils were prewetted by artificial rainfall prior to overland flow initiation. Overland flow was released from a concentrated source centered 4 m upslope of the plot discharge outlet. Each flow release rate was applied for 12 min using a flow regulator. In the early experiments (before 2006), the flow release rates were 3, 7, 12, 15, 21, 24 (L min^{-1}), while they were 15, 30, 45 (L min^{-1}) in the later experiments. The exception was the Breaks site in 2004, in which the flow release rates were 3, 7, 12, 15, 21, 24, 48 (L min^{-1}). The plot flow velocity for each flow release rate was measured using a salt tracing method [*Pierson et al.*, 2007, 2008, 2009, 2010; *Moffet et al.* 2007]. A concentrated salt solution ($CaCl_2$) was released into the fastest flow path (as determined by visual tracer). The mean travel time of the peak of the salt solution between rill cross sections at transects 1 and 3 m downslope of the release point was monitored instantaneously with conductivity probes. Flow velocity was calculated as the distance between conductivity probes (2 m) divided by the mean travel time of the salt solution between the 1 and 3 m transects.

[11] The width and depth of each flow path for each rate were measured at several transects along the slope. The number and locations of transects varied within sites where the minimum was two transects, one at 1 m and one at 3 m downslope of flow release point. Only the flow dimension measurements at transects 1 and 3 m were used in this study, in order to be consistent with the velocity measurements. At sites that had measurements at transects 0.5, 1.5, 2.5, 3.5 m only measurements at 1.5 and 2.5 m were considered. The flow path cross section was assumed to be rectangular for computational purposes [*Al-Hamdan et al.*, 2012]. Multiple depth measurements were taken for each cross section where the depth was calculated as the average of these measurements. The average width, depth, and hydraulic radius (R_h) of each flow path for each flow release

Table 2. Fraction of Surface (0–4 cm) Soil in Percentage Represented by Sand, Silt, and Clay (by Microsite and/or Treatment Where Specified) at Each Study Site

Site	Microsite	Treatment	% Sand	% Silt	% Clay
Breaks			73	24	3
Castlehead	Coppice		64	33	3
	Shrub-interspace	Burned	55	39	6
		Unburned	46	49	5
Denio		Burned	83.5	10	6.5
		Unburned	68.6	24.3	7.1
Marking Corral			66	30	4
Onaqui			56	37	7
Steens		Cut	45.2	37.5	17.3
		Uncut	46	38.8	15.2
Upper Sheep	Low Sagebrush		30	52	18
	Big Sagebrush		55.9	30.6	13.5

rate was then calculated as the average of means from each cross section. R_h was calculated as

$$R_h = \frac{wd}{(w + 2d)}, \tag{9}$$

where w (m) and d (m) are the average width and the average depth of each flow path, respectively. Then hydraulic radius assigned for each flow release experiment was calculated as the average value of R_h for all flow paths and the assigned width for the experiment was calculated as the sum of widths of all flow paths.

[12] The overland flow discharge for each experimental run was calculated as the average of the flow release rate and the outflow rate of a plot [see *Al-Hamdan et al.*, 2012]. While the flow release rate was controlled and measured by the flow regulator, the outflow discharge rate was derived from timed runoff samples which were collected in bottles or buckets at the exit of the plot [see *Pierson et al.*, 2007, 2008, 2009, 2010]. The outflow discharge rate was calculated as the sample volume divided by the collection time. An average outflow discharge rate for each experimental run was derived as the mean of the respective run samples. The timed runoff samples were weighed, oven-dried at 105°C then reweighed in order to estimate sediment concentration of runoff.

[13] The measured detachment capacity for each experimental run was calculated using an approximated solution of equation (8). The solution assumes that the change in D_r along the downslope distance of the plot is linear. The sediment transport rate G has a zero value at the flow release point and maximum value at the outlet of the plot. The solution resulted in the following equation:

$$D_{cf} = \frac{D_r}{\left(1 - 0.5\left(\frac{G_e}{T_c}\right)\right)} = \frac{\frac{G_e}{wl}}{\left(1 - 0.5\left(\frac{G_e}{T_c}\right)\right)}, \tag{10}$$

where w is the width (m) of concentrated flow, G_e is the measured sediment transport rate (kg s^{-1}) at the exit collected by the samples, and l is the length of the plot (4 m). Transport capacity (T_c) (kg s^{-1}) was calculated using the following logistic equation which was developed by *Nearing et al.* [1997]

$$\mathrm{Log}\left(\frac{10T_c}{w}\right) = -34.47 + 38.61 * \frac{\exp\left[0.845 + 0.412\log\left(1000\omega\right)\right]}{1 + \exp\left[0.845 + 0.412\log\left(1000\omega\right)\right]}, \tag{11}$$

where w is the width (m) of concentrated flow, and ω is the stream power (kg s^{-3}).

[14] The hydraulic parameters τ_s, ω, Ω, Γ, and q were calculated using equations (2) through (6). The fraction of soil friction to total friction (f_s/f_t) was calculated by the following equation [see *Al-Hamdan et al.*, 2011]:

$$\left(\frac{f_s}{f_t}\right) = 0.035\exp(3.41bare), \tag{12}$$

where *bare* is the fraction of bare soil area to the total ground area.

[15] To solve for K_{HP} and HP_c in equation (7), values of detachment capacity (D_{cf}) were plotted against the hydraulic parameters τ_s, ω, Ω, Γ, and q. The slope of the relationship between D_{cf} and each hydraulic parameter was considered equal to the K_{HP}, and the x axis intercept is equal to HP_c [*Cochrane and Flanagan*, 1997; *Moffet et al.*, 2007].

[16] *Foltz et al.* [2008] developed an exponential function of cumulative flow depth to describe the decrease of erodibility on native surface roads within overland flow events. Their selection of an exponential function was based on results from many studies that suggested erosion rates decreased in an exponential manner during overland flow events [e.g., *Megahan*, 1974; *Ziegler et al.*, 2002]. Results obtained from previous research work on sites used in our study show the same pattern of decaying sediment concentration [e.g., *Moffet et al.*, 2007; *Pierson et al.*, 2008]. Following *Foltz et al.* [2008], we hypothesized that concentrated flow erodibility K_{HP} decreases exponentially with cumulative unit width overland flow. However, unlike *Foltz et al.* [2008], who found a single decay factor along all the sequences of their overland flow experimental runs, we considered the variability within each experimental run (i.e., each experimental run has its own decay function). The equation that represents the temporal variability of erodibility K used here was an exponential decay function:

$$K = K_{(\mathrm{Max})}\exp\left(\beta q_c\right), \tag{13}$$

where $K_{(\mathrm{Max})}$ is the maximum measured erodibility within a flow release rate experimental run, q_c is the cumulative unit flow discharge (m^2), and β is the decay factor (m^{-2}). Values of K at each time step (i.e., time at which runoff samples were collected) within each flow release experiment was calculated using the forms of equation (7) that best fit our data. The decay factor β was calculated as the slope of the relationship between the values of log transformed K and the values of q_c. Since different flow release rates often resulted in different $K_{(\mathrm{Max})}$ values for the same plot, only one flow release rate which resulted in the maximum $K_{(\mathrm{Max})}$ was used for estimating the plot erodibility decay function. In most of the experiments, $K_{(\mathrm{Max})}$ was measured just after the start of the flow release, otherwise, points before $K_{(\mathrm{Max})}$ were dropped and the cumulative unit flow discharge was set to start adding up when erodibility is equal to $K_{(\mathrm{Max})}$ (i.e., $q_c = 0$ at $K = K_{(\mathrm{Max})}$). Finally, for purposes of parameterization of erodibility, average values of erodibility for each plot and flow release rate were also calculated.

3.3. Statistical Analysis

[17] SAS software [*SAS*, 2007] was used for all statistical analyses. Regression analysis between measured D_{cf} and each of the five measured hydraulic parameters was used to develop the linear relationship form of equation (7). Also, regression analysis between log transformed D_{cf} and the log transformations of each measured hydraulic parameter was used to develop the power law relationship form of equation (1). A very small value (1×10^{-23}) was added to D_{cf} in order to allow log transforming zero values. Regression

analysis between natural log transformed K for each sample of the flow release rate experiments and q_c was used to develop the erodibility decay function. Comparisons between erodibility values within treatments were based on median values. Multiple stepwise linear regression analysis was used to derive all the relationships between the erodibility factor and attributes of vegetation and ground cover. Prior to this analysis, values of K were log transformed (base 10) to address deviation from normality as well as to improve homoscedasticity and linearity [*Allison*, 1999]. A t test was used to test if the power law exponent (α) in equation (1) was significantly different from unity or not. A significance level of 0.05 was used for all statistical tests, including the criteria for including the variables in the multiple regressions.

4. Results and Discussion

4.1. Hydraulic Parameters and Detachment Capacity

[18] The flow shear stress values in the experiments varied from 0.07 to 39.7 Pa (kg s^{-2} m^{-1}), the stream power values varied from 0.05 to 17.4 J m^{-2} s^{-1} (kg s^{-3}), the unit stream power varied from 0.04×10^{-2} to 14.23×10^{-2} m s^{-1}, the unit length shear force varied from 0.838 to 235.3 kg s^{-2}, and the unit width discharge varied from 0.2×10^{-4} to 60×10^{-4} m^2 s^{-1}. The average values of hydraulic parameters among the different treatment or burn years were nearly consistent, except for shear stress, where generally more shear stress was applied on burned plots because of the higher percentage of bare soil, and hence, a lower fraction of shear stress was dissipated on vegetative roughness. Detachment capacity varied from near 0 to 0.068 kg s^{-1} m^{-2} and was generally highest at burned sites. The transport capacity per unit width varied from 0.0002 to 3.03 kg s^{-1} m^{-1}. The values of measured sediment transport rate to transport capacity ratio were low, with an average of 6.7%, which indicated that the erosion process in the experiments was not limited in general by transport capacity.

4.2. Relationship Comparison

[19] In the linear relations, none of the hydraulic parameters consistently predicted the detachment capacity well for all sites (Table 3). Shear stress was the best predictor in most data when combined into one set for each study site.

Table 3. Concentrated Flow Erodibility Coefficients Based on Stream Power (K_ω), Unit Stream Power (K_Ω), Unit Length Shear Force (K_Γ), Flow Shear Stress (K_{τ_s}), and Unit Discharge (K_q) for the Linear Model of Equation (7), Calculated as the Slope of Linear Regression Between Average Detachment Capacity and Each of the Five Hydraulic Parameters for All Sites and Treatments[a]

Site	Treatment	Year(s)	n	K_ω (s^2 m^{-2}) $\times 10^{-3}$	R^2	K_Ω (kg m^{-3}) $\times 10^{-1}$	R^2	K_Γ (s m^{-2}) $\times 10^{-3}$	R^2	K_{τ_s} (s m^{-1}) $\times 10^{-3}$	R^2	K_q (kg m^{-4})	R^2
Breaks	All	All	66	**0.968**	0.12	0.574	0.05	Negative	–	**1.004**	0.38	**4.048**	0.12
	Burned	All	60	**0.968**	0.12	0.562	0.05	Negative	–	**1.064**	0.4	**4.061**	0.12
	Burned	0	8	**4.297**	0.69	5.497	0.44	Negative	–	1.079	0.5	**18.113**	0.72
	Burned	1	8	Negative	–	Negative	–	0.454	0.11	**1.220**	0.52	Negative	–
	Burned	2	23	**1.535**	0.25	**3.86**	0.48	Negative	–	**1.657**	0.34	**8.392**	0.32
	Burned	3	21	**0.035**	0.31	0.010	0.08	Negative	–	0.003	0.004	**0.145**	0.34
	Unburned	All	6	0.918	0.18	0.983	0.09	Negative	–	1.897	0.06	3.932	0.20
Castlehead	All	All	28	**5.96**	0.65	**10.46***	0.72	Negative	–	Negative	–	**10.265**	0.67
	Burned	1	12	**2.497**	0.80	**3.137***	0.89	Negative	–	0.394	0.14	4.405	0.75
	Unburned	All	16	**5.925**	0.60	**11.26**	0.73	Negative	–	**8.954**	0.25	**10.178**	0.62
Denio	All	All	109	0.078	0.002	Negative	–	Negative	–	**0.604***	0.68	0.925	0.01
	Burned	All	71	**4.37***	0.53	**1.977**	0.08	Negative	–	**0.608**	0.64	**13.189***	0.50
	Burned	0	18	**5.343**	0.85	**7.702**	0.57	Negative	–	**1.067**	0.47	**17.094**	0.84
	Burned	1	20	1.571	0.14	0.936	0.06	Negative	–	0.635	0.16	4.909	0.15
	Burned	2	18	0.268	0.14	Negative	–	Negative	–	0.085	0.11	0.979	0.17
	Burned	3	15	**0.457**	0.34	0.179	0.08	Negative	–	**0.750**	0.27	**1.426**	0.42
	Unburned	All	38	**0.013**	0.39	**0.012**	0.19	Negative	–	0.033	0.04	**0.049**	0.41
Marking Corral	All	All	58	**6.009***	0.56	**1.61**	0.08	Negative	–	**1.418**	0.23	**5.026***	0.34
	Burned	All	24	**8.004***	0.83	**10.091***	0.66	Negative	–	**1.529**	0.19	**8.863***	0.68
	Burned	1	12	**8.918***	0.87	**11.222***	0.86	Negative	–	**1.848**	0.35	**11.692***	0.76
	Burned	2	12	**7.017***	0.77	**8.592**	0.38	Negative	–	0.343	0.01	**7.019**	0.65
	Unburned	All	34	0.74	0.02	Negative	–	Negative	–	**1.066**	0.35	0.354	0.01
Onaqui	All	All	80	**0.947**	0.12	**0.540**	0.05	0.018	0.005	**0.979***	0.48	1.089	0.06
	Burned	All	23	**3.763**	0.49	**2.466**	0.22	Negative	–	**1.707***	0.81	**11.337***	0.64
	Burned	1	11	2.409	0.19	**1.866**	0.16	Negative	–	**1.650***	0.67	**8.871**	0.48
	Burned	2	12	**4.582**	0.74	**3.149**	0.3	0.238	0.11	**1.788***	0.92	**13.621***	0.79
	Unburned	All	57	**0.337**	0.11	0.161*	0.03	Negative	–	Negative	–	**0.66**	0.16
Steens	All	All	16	**0.082**	0.09	0.007	0.001	Negative	–	0.008	0.08	0.166	0.11
	Cut	All	8	0.179	0.44	0.105	0.17	Negative	–	Negative	–	0.293	0.4
	Uncut	All	8	**0.231**	0.81	0.205	0.33	Negative	–	Negative	–	**0.45**	0.86
Upper Sheep (Big Sagebrush)	All	All	24	**1.334**	0.31	0.206	0.01	Negative	–	**0.799**	0.50	**4.124**	0.28
	Burned	1	12	**0.772**	0.19	0.286	0.01	0.007	0.003	0.198	0.04	2.503	0.18
	Unburned	All	12	0.109	0.20	0.07	0.23	Negative	–	Negative	–	0.268	0.13
Upper Sheep (Low Sagebrush)	All	All	12	0.615	0.24	**1.265**	0.39	Negative	–	0.294	0.20	0.566	0.07
	Burned	1	4	0.151	0.01	2.152	0.42	Negative	–	Negative	–	0.68	0.03
	Unburned	All	8	**0.206**	0.77	0.307	0.66	Negative	–	0.135	0.16	**0.286**	0.7
All data			393	**0.742**	0.09	**0.527**	0.03	Negative	–	**0.572**	0.29	**3.919**	0.17

[a]Bold indicates the coefficient was significantly different than 0 ($\alpha = 0.05$). Values marked with * means the model critical value (HP_c) is significantly higher than 0 ($\alpha = 0.05$).

However, when treatment classes were considered, shear stress did not perform well especially on the less erodible, undisturbed plots. When each experimental year was considered separately, stream power performed very well, especially at recently burned sites. The unit flow discharge followed the same pattern as stream power. Performance of unit stream power did not follow any trend as it was a good predictor at some sites and was the opposite at other sites. Unit length shear force performed poorly at all sites as all of the relationships produced values of erodibility that were either negative or not significantly positive. Regardless which hydraulic indicator was used, the critical value (HP_c) was either negative or insignificant when all the sites and treatments were combined. Critical values were also negative or insignificant in most cases when considering study or treatment classes.

[20] Log transformed regression (power law relationship) did not improve the predictions regardless which hydraulic parameter was used (Table 4). Values of power law exponent (α) in equation (1) were not consistent among study sites or treatments. The power law exponent varied from negative values to 2.57 when using stream power and from negative to 2.38 when using shear stress. In most of the study sites, the power law exponent for stream power, unit stream power, and unit flow discharge have higher values in combined burned sites than in unburned sites. The average value of the power law exponent among different treatments and years ($n = 24$) was 1.18 for stream power, 0.92 for unit stream power, 0.67 for shear stress, and 1.29 for unit discharge. A t test showed that none of these power law exponents were significantly different from 1 ($\alpha = 0.05$).

[21] The low R^2 in the linear and power law relations for hydraulic parameters such as shear stress and stream power in undisturbed sites could be due to the ground cover. More cover could increase the variability of how the cover acts to protect the soil. The poor performance of unit length shear force could be explained by the fact that the parameter estimate depends totally on flow cross section area, which is very hard to measure accurately in the field given the dynamic change of cross section shape during runoff. Improving the measurement of the area and shape of the concentrated flow cross section would improve the performance of the four hydraulic parameters that depend on flow geometry (stream power, unit length shear force, flow shear stress, and unit discharge).

Table 4. Power-Law Exponents of Equation (1) for Concentrated Flow Erodibility Based on Stream Power (K_ω), Unit Stream Power (K_Ω), Unit Length Shear Force (K_Γ), Flow Shear Stress (K_{τ_s}), and Unit Discharge (K_q) With $HP_c = 0$, Calculated as the Slope of Regression Between Log of Average Detachment Capacity and Log of Each of the Five Hydraulic Parameters for All Sites and Disturbance Presented in This Paper

Site	Treatment	Year(s)	n	K_ω	R^2	K_Ω	R^2	K_Γ	R^2	K_{τ_s}	R^2	K_q	R^2
Breaks	All	All	66	1.3	0.12	1.07	0.1	Negative	–	1.83	0.31	1.3	0.11
	Burned	All	60	1.49	0.21	1.23	0.18	Negative	–	1.71	0.33	1.53	0.2
	Burned	0	8	1.87	0.59	1.83	0.31	Negative	–	1.29	0.32	2.18	0.60
	Burned	1	8	Negative	–	Negative	–	0.66	0.19	0.96	0.21	Negative	–
	Burned	2	23	1.36	0.41	1.29	0.29	0.78	0.18	2.02	0.68	1.48	0.39
	Burned	3	21	1.01	0.61	0.54	0.28	Negative	–	Negative	–	1.05	0.62
	Unburned	All	6	Negative	–	Negative	–	7.04	0.25	Negative	–	Negative	–
Castlehead	All	All	28	2.14	0.65	2.28	0.56	Negative	–	0.90	0.13	2.22	0.61
	Burned	1	12	2.12	0.75	2.21	0.70	Negative	–	0.69	0.09	2.32	0.68
	Unburned	All	16	2.5	0.71	2.76	0.59	Negative	–	2.38	0.42	2.52	0.66
Denio	All	All	109	Negative	–	Negative	–	Negative	–	1.98	0.74	0.2	0.003
	Burned	All	71	2.57	0.32	0.75	0.03	Negative	–	1.72	0.70	2.64	0.3
	Burned	0	18	1.22	0.72	1.12	0.43	Negative	–	1.56	0.32	1.29	0.73
	Burned	1	20	1.22	0.20	0.79	0.10	Negative	–	1.29	0.12	1.34	0.21
	Burned	2	18	1.86	0.24	0.58	0.03	0.3	0.01	0.68	0.07	1.97	0.21
	Burned	3	15	0.81	0.05	0.26	0.01	Negative	–	0.36	0.003	0.80	0.05
	Unburned	All	38	1.00	0.36	0.92	0.19	Negative	–	2.06	0.22	1.04	0.36
Marking Corral	All	All	58	1.38	0.32	1	0.18	Negative	–	0.84	0.20	1.27	0.24
	Burned	All	24	1.77	0.52	2.2	0.54	Negative	–	0.88	0.11	1.81	0.44
	Burned	1	12	2.08	0.53	2.23	0.59	Negative	–	1.21	0.28	2.52	0.46
	Burned	2	12	1.57	0.51	2.14	0.45	Negative	–	0.30	0.01	1.53	0.44
	Unburned	All	34	0.81	0.1	0.35	0.03	Negative	–	0.99	0.40	0.62	0.06
Onaqui	All	All	80	0.80	0.24	0.63	0.15	Negative	–	0.64	0.19	0.76	0.17
	Burned	All	23	1.47	0. 45	1.05	0.24	Negative	–	2.16	0.71	2.18	0.5
	Burned	1	11	1.19	0.42	0.82	0.23	Negative	–	2.29	0.79	1.81	0.57
	Burned	2	12	1.82	0.50	1.41	0.28	1.19	0.06	2.17	0.68	2.90	0.49
	Unburned	All	57	0.64	0.26	0.45	0.12	Negative	–	0.10	0.01	0.77	0.29
Steens	All	All	16	Negative	–	Negative	–	Negative	–	1.68	0.15	Negative	–
	Cut	All	8	2.32	0.20	0.63	0.02	Negative	–	Negative	–	2.43	0.27
	Uncut	All	8	1.02	0.75	1.05	0.46	Negative	–	Negative	–	0.96	0.75
Upper Sheep	All	All	24	2.63	0.44	1.59	0.22	Negative	–	2.03	0.47	2.67	0.44
(Big Sagebrush)	Burned	1	12	0.27	0.16	0.12	0.03	0.01	0.001	0.16	0.07	0.22	0.09
	Unburned	All	12	1.67	0.73	1.09	0.63	Negative	–	Negative	–	1.65	0.7
Upper Sheep	All	All	12	1.63	0.61	1.73	0.65	Negative	–	1.96	0.53	1.41	0.35
(Low Sagebrush)	Burned	1	4	0.65	0.19	1.85	0.63	Negative	–	Negative	–	0.83	0.26
	Unburned	All	8	1.07	0.57	0.96	0.42	Negative	–	1.81	0.36	0.94	0.45
All data			393	0.64	0.1	0.5	0.05	0.02	–	1.03	0.27	1.1	0.12

[22] The variation of power law exponent values when using stream power and shear stress indicates that no exponent value was consistently good for modeling detachment capacity. This variation is evident in several studies in literature. For instance, *Nearing et al.* [1999] showed that the exponent for stream power is 2.043 while *Zhang et al.* [2003] showed a value of 1.07 for the same exponent. The negative or insignificant values of critical shear stress or critical stream power were also reported in different studies [e.g., *Moffet et al.*, 2007; *Wagenbrenner et al.*, 2010]. The fact that power law exponents are not significantly different from 1 and critical values are either negative or not significantly different from zero suggests equation (7) can be reduced, for this data, to a simple equation:

$$D_{cf} = K_{HP}(HP). \tag{14}$$

Since a critical or threshold value of either stream power or shear stress was not statistically discernible for most samples, we chose to use equation (14) to calculate the measured erodibility for each sample. Thus the equations for stream power and flow shear stress cases are

$$K_{\omega} = \frac{D_{cf}}{\omega}, \tag{15}$$

$$K_{\tau_s} = \frac{D_{cf}}{\tau_s}, \tag{16}$$

where K_{ω} is the stream power based erodibility ($s^2\ m^{-2}$) and K_{τ_s} is the flow shear stress based erodibility ($s\ m^{-1}$). An average erodibility factor for each flow release rate on each plot was calculated as the mean of the respective sample erodibility values.

4.3. Describing Temporal Variability of Erodibility Within an Overland Runoff Event

[23] The results show that concentrated flow erodibility calculated by equations (15) and (16) was not constant within each experimental flow release rate, but that in most cases erodibility was much higher at the beginning than at the end of the experimental run (see Figure 1). A regression between the natural log of erodibility and the cumulative unit flow rate was done for each plot. The maximum erodibility values varied among flow release rates for the same plot. Hence, one flow release rate (one with the highest maximum erodibility) for each plot was used for estimating the decay factor. Figure 1 shows an example of the regression. The average R^2 of the regressions for all plots was 0.56.

[24] The decay factor that describes the decrease of erodibility within an overland flow event is presented in Table 5. It can be seen that decay parameter did not have a general trend within years after treatment. The changes in concentrated erodibility over short time periods within a flow event can be attributed to ample detachable soil on recently disturbed conditions. In addition, as erosion progresses the bed of the concentrated flow path changes from a less cohesive soil layer to a more cohesive soil layer. Moreover, decreases in sediment concentration can be also explained by the increase of hydraulic roughness as a result of exposing larger soil aggregates. The increase of hydraulic roughness may reduce erosivity and transport capacity within the same flow rate [*Govers*, 1992; *Nearing et al.*, 1997]. However, this factor is less important in this study because in most cases runoff either increases with time or tends to be steady. The high negative values of decay factors in some plots can be explained by the fact that, in these plots, only a very small amount of detachable sediment was available at the top of soil surface, hence erodibility declined quickly to zero after winnowing.

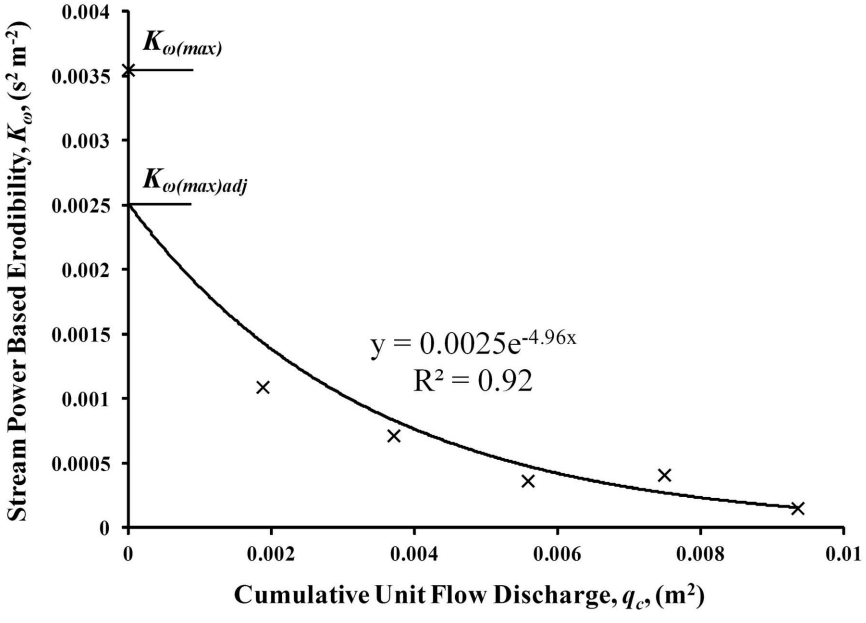

Figure 1. An example of an experimental run with erodibility started from maximum measured erodibility ($K_{\omega(\max)}$) before it decreases with time, and the regression of the erodibility as a function of cumulative unit width flow discharge; the intercept of the regression is the adjusted maximum erodibility ($K_{\omega(\max)adj}$).

Table 5. Mean and Median Values of the Decay Factor (β) of Equation (13) Using Stream Power Based and Flow Shear Stress Based Concentrated Flow Erodibility

			Stream Power Based β (m^{-2})			Flow Shear Stress Based β (m^{-2})		
Site	Treatment	Year(s)	*n*	Mean	Median	*n*	Mean	Median
Breaks	All	All	63	−6.39	−4.21	62	−5.02	-4.31
	Burned	All	58	−6.33	−4.28	58	−5.19	−4.47
	Burned	0	8	−13.43	−2.89	8	−3.98	−2.94
	Burned	1	6	−3.10	−2.85	6	−3.16	−2.84
	Burned	2	23	−4.58	−4.21	20	−4.80	−4.37
	Burned	3	21	−6.46	−5.36	22	−6.65	−5.27
	Unburned	All	5	−7.09	−2.09	4	−2.58	−2.66
Castlehead	All	All	24	−8.49	−4.12	25	−8.09	−4.22
	Burned	1	10	−15.29	−11.11	10	−14.91	−10.86
	Unburned	All	14	−3.63	−2.46	15	−3.54	−2.11
Denio	All	All	75	−9.47	−6.57	77	−8.25	−6.25
	Burned	All	47	−9.30	−7.78	49	−8.94	−7.62
	Burned	0	17	−9.62	−10.01	17	−9.15	−7.32
	Burned	2	16	−10.64	−9.88	17	−9.56	−9.59
	Burned	3	7	−7.38	−5.52	15	−7.99	−5.81
	Unburned	All	28	−9.76	−4.52	28	−7.05	−4.06
Marking Corral	All	All	46	−10.47	−6.10	48	−10.55	−5.95
	Burned	All	18	−16.35	−7.27	20	−15.66	−4.24
	Burned	1	10	−8.97	−7.27	10	−7.74	−4.24
	Burned	2	8	−25.57	−13.07	10	−23.58	−12.95
	Unburned	All	28	−6.69	−6.10	28	−6.90	−6.17
Onaqui	All	All	74	−4.56	−2.66	70	−4.60	−2.53
	Burned	All	23	−7.39	−6.58	23	−7.12	−5.97
	Burned	1	11	−7.80	−7.08	11	−7.83	−6.80
	Burned	2	12	−7.02	−5.91	12	−6.48	−5.62
	Unburned	All	51	−3.28	−1.84	47	−3.36	−1.80
Upper Sheep (Big Sagebrush)	All	All	23	−7.11	−4.73	23	−7.11	−4.28
	Burned	1	12	−5.86	−4.23	12	−5.62	−4.00
	Unburned	All	11	−8.47	−5.21	11	−8.73	−5.76
Upper Sheep (Low Sagebrush)	All	All	11	−16.25	−12.63	10	−13.91	−12.2
	Burned	1	3	−10.78	−15.05	3	−9.89	−14.18
	Unburned	All	8	−18.30	−11.72	7	−16.63	−10.23
All sites			316	−7.84	−4.8	315	−7.24	−4.72

4.4. Erodibility Estimates and Disturbance Impact

[25] In general, maximum erodibility values calculated by equations (15) and (16) were greater for burned plots than nonburned plots at a site (Table 6). In addition, erodibility was significantly reduced 10 years following tree removal at the Steens site. Calculated average erodibility of each plot also showed the same pattern as maximum erodibility, but with more variation of the values within each treatment year (Table 6). Average value of K_{τ_s} for all plots ($n = 393$) was 0.00087 s m^{-1} which is in the range of 0.00004 to 0.00302 s m^{-1} reported by *Laflen et al.* [1991] for rangelands and slightly less than the range of 0.00117 to 0.02413 s m^{-1} for cropland reported by the same authors. The average value of maximum stream power based erodibility K_ω was 0.00169 s^2 m^{-2} which is slightly less than the range of 0.0022 to 0.04896 s^2 m^{-2} for agricultural soils reported by *Elliot and Laflen* [1993].

[26] Fire effects on erodibility varied among study sites and were most evident for Breaks, Denio, Upper Sheep, and Onaqui (Table 6). Fire impact on erodibility at the Castlehead and Marking Corral sites initially shows an atypical postdisturbance trend, where erodibility was higher for unburned conditions. However analysis by microsite (shrub-interspaces versus coppices) shows that burned coppice plots have significantly higher values than unburned coppice plots (Table 7).

[27] The degree of fire impact on erodibility at a site was strongly affected by prefire vegetation and ground cover distribution and their respective influence on burn severity and prefire site degradation (Tables 6–8). Dense prefire vegetation and litter cover on the sagebrush steppe sites (Denio, Breaks, and Upper Sheep, Table 8) likely promoted aggregate stability and protected the soil surface against the erosive force of overland flow. Densely vegetated surfaces in semiarid climates contribute organic matter to the soil profile and recruit soil fauna activity [*Belnap et al.*, 2005]; both of which improve soil structure and promote infiltration and soil retention [*Blackburn et al.*, 1990; *Ludwig et al.*, 2005]. Although vegetation contributed to low erodibility on the sagebrush sites prefire (Table 6), the density of cover provided a high quantity and continuity of fuels that promoted high fire severity. For instance, burning amplified erodibility on Denio sites by 500-fold (Table 6). Severe burning affects soil erodibility by reducing soil-binding organic matter [*Giovannini et al.*, 1988; *DeBano*, 1991; *DeBano et al.*, 1998; *Ubeda and Outeiro*, 2009] and by reducing the root density in upper soil layer. Plant roots increase soil cohesion and hence reduce erodibility by overland flow [*Gyssels et al.*, 2005; *De Baets et al.*, 2006; *De Baets and Poesen*, 2010). Fire removal of dense vegetation further amplifies soil loss by decreasing rainfall and overland flow interception/storage, resulting in generation

Table 6. Mean and (Median) Values of the Average and Maximum Stream Power Concentrated Flow Erodibility Coefficients K_ω, Calculated By Equation (15) and Mean and (Median) Values of Average and Maximum of Flow Shear Stress Concentrated Flow Erodibility Coefficients K_{τ_s}, Calculated By Equation (16) for All Sites and Treatments in This Study

				K_ω ($s^2\ m^{-2}$) $\times 10^{-3}$		K_{τ_s} ($s\ m^{-1}$) $\times 10^{-3}$	
Site	Treatment	Year(s)	n	Average	Maximum	Average	Maximum
Breaks	All	All	66	0.88 (0.39)	2.48 (0.97)	0.61 (0.38)	2.49 (1.24)
	Burned	All	60	0.92 (0.48)	9.31 (6.93)	0.58 (0.39)	2.38 (1.24)
	Burned	0	8	2.09 (1.29)	5.05 (3.64)	0.66 (0.51)	2.48 (2.02)
	Burned	1	8	1.97 (1.72)	4.82 (4.11)	1.00 (0.87)	4.75 (3.42)
	Burned	2	23	0.94 (0.65)	3.30 (1.58)	0.86 (0.57)	3.31 (1.71)
	Burned	3	21	0.05 (0.04)	0.16 (0.12)	0.08 (0.51)	0.40 (0.13)
	Unburned	All	6	0.51 (0.19)	0.90 (0.38)	0.96 (0.16)	3.61 (1.07)
Castlehead	All	All	28	7.61 (2.20)	41.85 (6.80)	5.73 (0.83)	69.13 (7.52)
	Burned	1	12	2.11(1.93)	9.31 (6.93)	0.51 (0.35)	4.19 (2.79)
	Unburned	All	16	11.72 (2.40)	66.25 (6.80)	9.65 (3.55)	117.83 (24.24)
Denio	All	All	109	0.99 (0.09)	3.15 (0.30)	0.23 (0.07)	1.09 (0.44)
	Burned	All	71	1.52 (0.53)	4.82 (1.41)	0.33 (0.22)	1.60 (0.93)
	Burned	0	18	3.83 (3.43)	13.95 (11.59)	0.49 (0.41)	2.61 (2.42)
	Burned	1	20	1.66 (1.18)	3.48 (2.26)	0.49 (0.42)	2.13 (1.44)
	Burned	2	18	0.23 (0.16)	0.99 (0.64)	0.15 (0.08)	0.87 (0.54)
	Burned	3	15	0.10 (0.05)	0.25 (0.16)	0.15 (0.06)	0.56 (0.22)
	Unburned	All	38	0.011 (0.007)	0.037 (0.02)	0.04 (0.02)	0.14 (0.06)
Marking Corral	All	All	58	2.57 (0.95)	8.18 (1.64)	0.79 (0.30)	4.69 (1.46)
	Burned	All	24	2.29(0.65)	6.2 (1.29)	0.94 (0.11)	4.48 (0.44)
	Burned	1	12	3.01 (1.62)	8.39 (2.93)	1.09 (0.31)	5.38 (1.23)
	Burned	2	12	1.57 (0.39)	4.02 (0.91)	0.71(0.08)	3.57 (0.28)
	Unburned	All	34	2.77 (1.00)	11.28 (1.67)	0.69 (0.38)	4.85 (1.87)
Onaqui	All	All	80	1.15 (0.64)	3.65 (1.16)	0.63 (0.35)	3.15 (0.88)
	Burned	All	23	2.27 (1.05)	8.26 (3.37)	0.49 (0.35)	2.80 (1.58)
	Burned	1	11	2.19 (0.95)	8.52 (1.70)	0.44 (0.23)	2.92 (1.01)
	Burned	2	12	2.33 (1.73)	8.01 (5.12)	0.53 (0.37)	2.68 (1.85)
	Unburned	All	57	0.71 (0.57)	1.79 (1.03)	0.69 (0.33)	3.29 (0.76)
Steens	All	All	16	0.11 (0.12)	0.2 (0.24)	0.010 (0.005)	0.028 (0.018)
	Cut	All	8	0.031 (0.009)	0.057 (0.013)	0.007 (0.002)	0.016 (0.023)
	Uncut	All	8	0.19 (0.203)	0.348 (0.303)	0.013 (0.010)	0.041 (0.032)
Upper Sheep	All	All	24	1.24 (0.78)	3.45 (3.08)	0.66 (0.49)	3.20 (2.58)
(Big Sagebrush)	Burned	1	12	2.37 (1.94)	6.43 (4.97)	1.15 (0.93)	5.20 (4.20)
	Unburned	All	12	0.12 (0.04)	0.47 (0.12)	0.16 (0.04)	1.19 (0.14)
Upper Sheep	All	All	12	0.95 (0.24)	2.17 (0.91)	0.25 (0.13)	1.04 (0.76)
(Low Sagebrush)	Burned	1	4	2.44 (1.89)	4.82 (4.8)	0.54 (0.52)	2.07 (2.09)
	Unburned	All	8	0.2 (0.19)	0.85 (0.58)	0.11 (0.10)	0.53 (0.48)
All data			393	1.69 (0.52)	6.65 (1.05)	0.87 (0.24)	7.21 (0.89)

Table 7. Mean and (Median) of the Average and Maximum Stream Power Concentrated Flow Erodibility Coefficients K_ω ($s^2\ m^{-2}$) $\times 10^{-3}$, Calculated by Equation (15) for Castlehead, Marking Corral, and Onaqui Sites Where Data Divided Into Two Microsites: (a) Coppice Area and (b) Shrub-Interspace Area

			Coppice Area			Shrub-Interspace Area		
Site	Treatment	Year(s)	Average	Maximum	n	Average	Maximum	n
Castlehead	All	All	2.31 (2.56)	10.74 (10.98)	9	10.12 (2.18)	56.59 (5.58)	19
	Burned	1	3.04 (3.20)	14.67 (15.74)	6	1.19 (1.03)	3.96 (3.67)	6
	Unburned	All	0.83 (0.11)	2.89 (3.89)	3	14.24 (4.32)	80.88 (8.59)	13
Marking Corral	All	All	1.71 (0.2)	4.52 (0.53)	18	2.96 (1.05)	11.28 (1.82)	40
	Burned	All	2.34 (0.37)	6.05 (0.77)	12	2.22 (0.86)	6.35 (1.63)	12
	Burned	1	2.10 (1.18)	5.57 (2.03)	6	3.93 (2.61)	11.21 (4.70)	6
	Burned	2	2.6 (0.2)	6.54 (0.53)	6	0.53 (0.56)	1.50 (1.22)	6
	Unburned	All	0.44 (0.09)	1.45 (0.28)	6	3.27 (1.11)	13.39 (1.83)	28
Onaqui	All	All	1.98 (0.78)	7.79 (2.71)	26	0.76 (0.59)	1.65 (1.05)	54
	Burned	All	3.63 (1.68)	14.55 (5.61)	11	1.01 (0.83)	2.49 (1.73)	12
	Burned	1	4.03 (1.18)	17.15 (5.24)	5	0.66 (0.64)	1.34 (1.11)	6
	Burned	2	3.30 (2.82)	12.38 (10.46)	6	1.37 (1.10)	3.64 (3.06)	6
	Unburned	All	0.77 (0.53)	2.83 (1.14)	15	0.68 (0.57)	1.42 (1.03)	42
All data			1.95 (0.84)	7.18 (2.81)	53	3.11 (0.73)	14.30 (1.56)	113

Table 8. Mean and (Median) of Plant Residue Cover and Basal Plant and Cryptogam Cover for Each Site and Treatment in This Study

Site	Treatment	Year(s)	*n*	Residue	Basal Plant and Cryptogam
Breaks	Burned	0	8	0.23 (0.26)	0.001 (0.001)
	Burned	1	8	0.30 (0.26)	0.02 (0.02)
	Burned	2	23	0.44 (0.43)	0.08 (0.06)
	Burned	3	21	0.58 (0.56)	0.05 (0.04)
	Unburned	All	6	0.71 (0.71)	0.01 (0.02)
Castlehead	Burned	1	12	0.18 (0.15)	0.01 (0.01)
	Unburned	All	16	0.23 (0.08)	0.04 (0.04)
Denio	Burned	0	18	0.02 (0.02)	0.02 (0.02)
	Burned	1	20	0.21 (0.21)	0.11 (0.10)
	Burned	2	18	0.31 (0.25)	0.28 (0.28)
	Burned	3	15	0.39 (0.38)	0.40 (0.40)
	Unburned	All	38	0.47 (0.44)	0.44 (0.45)
Marking Corral	Burned	1	12	0.41 (0.33)	0.01 (0.02)
	Burned	2	12	0.44 (0.45)	0.02 (0.02)
	Unburned	All	34	0.46 (0.37)	0.04 (0.03)
Onaqui	Burned	1	11	0.19 (0.17)	0.02 (0.01)
	Burned	2	12	0.29 (0.26)	0.02 (0.01)
	Unburned	All	57	0.37 (0.14)	0.08 (0.05)
Steens	Cut	All	8	0.27 (0.28)	0.04 (0.04)
	Uncut	All	8	0.09 (0.07)	0.01 (0.01)
Upper Sheep (Big Sagebrush)	Burned	1	12	0.51 (0.48)	0.03 (0.03)
	Unburned	All	12	0.83 (0.85)	0.13 (0.13)
Upper Sheep (Low Sagebrush)	Burned	1	4	0.27 (0.25)	0.32 (0.34)
	Unburned	All	8	0.32 (0.31)	0.30 (0.28)

of high-velocity concentrated flow [*Pierson et al.*, 2001, 2002; *Snyman*, 2003; *Pierson et al.*, 2008, 2009]. High velocity, concentrated flow on bare soil amplifies erosive forces applied at the soil surface, resulting in increased surface erosion.

[28] Fire impacts on erodibility at wooded shrublands (Castlehead, Marking Corral, and Onaqui) varied with prefire cover conditions (Tables 6 and 7). Tree encroachment and infill on semiarid rangelands commonly result in degraded shrub-interspace areas with minimal plant cover and decreased surface soil aggregate stability [*Miller et al.*, 2000, 2005; *Pierson et al.*, 2007, 2010]. Prefire erodibility from shrub-interspaces at tree encroached sites in this study was generally high relative to tree coppices (Table 7) and the well vegetated sagebrush sites (Table 6). With exception of Castlehead, burning had minimal impact on erodibility from wooded-shrubland interspaces (Table 7) due to degraded prefire conditions; erodibility was high prefire and fuel conditions resulted in low burn severity. Low fuel density in woodland shrub-interspaces typically inhibits burning and results in low severity fire impacts between tree canopies. In contrast, thick litter mats underneath tree canopies [i.e., *Pierson et al.*, 2010] promote high fire severity and result in intense burning at the soil surface and extensive bare ground postfire. Fire removal of surface litter on tree coppices exposes a new source of highly erodible sediment. Burning increased bare soil and surface soil erodibility significantly on tree coppices at wooded-shrublands sites (Table 7). The immediate effect of burning on wooded shrublands is an increase in erodibility in areas previously covered by tree canopy and enhanced connectivity of highly erodible shrub-interspace and burned tree coppice microsites. Fire may however reduce long-term soil erodibility from tree-encroached sites where burning promotes shrub and herbaceous recruitment. The dramatic reduction in erodibility in shrub-interspaces at Castlehead one year postfire is likely due to the extensive recruitment of shrub-interspace herbaceous cover (threefold increase). The reduction of erodibility in the shrub-interspace at the Steens site 10 years following the cut treatment is attributed to shrub and herbaceous plant recruitment postcutting.

4.5. Describing Temporal Variability of Erodibility Within Recovery Period

[29] The erodibility pattern with time (years since fire) was associated with the degree of fire impact, vegetation recovery, and probably soil characteristics of the sites. Fire at Denio removed nearly all of the vegetation and ground cover and greatly amplified soil erodibility and soil exposure in the immediate postfire period. Erodibility at Denio remained higher on burned plots than nonburned plots until the third year postfire, when vegetation cover returned to near prefire levels. On the other hand, fire at the Breaks site was less severe and left some plant residue on the ground. The reduced fire severity at the Breaks site may explain the delayed increase in erodibility. Weathering of the exposed soil surface during the first year postfire likely reduced aggregate stability on burned areas at the Breaks site. A multiple regression equation between the logarithm of erodibility as a dependent variable and vegetation cover and rock cover as independent variables was developed for predicting the change of erodibility for different vegetation recovery levels. The results of log-transformed regression showed that stream power erodibility decreased as litter, basal plant and cryptogam, and rock cover increased (Table 9) while shear stress erodibility decreased as litter and basal plant cover increased and rock cover decreased (Table 10). The Onaqui site was an exception where litter correlated positively with flow shear stress erodibility. Vegetation cover variables have better performance in predicting stream power erodibility than in predicting flow shear stress erodibility. The equations in Tables 9 show that K_ω variability within years after disturbance can be predicted from vegetation cover variables associated with recovery of each site.

[30] All cover attributes can reduce concentrated flow erosion by reducing the erosive force fraction applied on soil. Organic material represented by litter amount and root density represented by basal plant as indicator of root density, increased soil cohesion, and reduced erodibility. The increase of rock was an indicator of vegetation reduction and consequently an increase of shear stress erodibility. The results agree with *Knapen et al.* [2008] who showed that the dry mass of organic material in the topsoil (i.e., roots and crop residue) is an important variable to predict concentrated flow erodibility, while plant residue can be indicative of organic matter added to the soil. The predictive equations developed could potentially be improved by including more variables such as soil moisture, dry soil bulk density, microbiotic crust cover, and/or dry mass of organic material in the topsoil [*Knapen et al.* 2007b; *Knapen and Poesen*, 2010], however, these variables are not as commonly measured and reported by rangeland managers and researchers as those used in this study.

4.6. Modeling Implications

[31] For undisturbed rangeland as well as sites disturbed by tree encroachment, estimated average erodibility values

Table 9. Multiple Regressions Equations for Estimating the Average K_w ($s^2\ m^{-2}$), and Maximum Values $K_{\omega(\mathrm{Max})}$ ($s^2\ m^{-2}$), of Stream Power Based Concentrated Flow Erodibility Coefficients as a Function of Basal Plant and Cryptogam Cover (*bascry*), Plant Litter (*res*), and Rock Cover (*rock*) for Each Site in This Study

Equation	n	R^2
Breaks		
$\log(K_w) = -2.02 - 3.30res$	66	0.47
$\log(K_{\omega(\mathrm{Max})}) = -1.57 - 3.36res$	66	0.48
Castlehead		
$\log(K_\omega) = -2.41 - 1.30res$	28	0.21
$\log(K_{\omega(\mathrm{Max})}) = -1.71 - 15.24bascry$	28	0.24
Denio		
$\log(K_\omega) = -2.21 - 2.58res - 3.50bascry$	109	0.81
$\log(K_{\omega(\mathrm{Max})}) = -1.75 - 2.70res - 3.35bascry$	109	0.77
Marking Corral		
$\log(K_\omega) = -2.3 - 1.31res - 1.57rock$	58	0.18
$\log(K_{\omega(\mathrm{Max})}) = -1.95 - 1.28res - 1.50rock$	58	0.19
Onaqui		
$\log(K_\omega) = -2.55 - 0.83rock - 1.77bascry$	80	0.25
$\log(K_{\omega(\mathrm{Max})}) = -2.74 - 2.02bascry$	80	0.08
Steens		
$\log(K_\omega) = -3.61 - 4.25res$	16	0.37
$\log(K_{\omega(\mathrm{Max})}) = -3.32 - 4.46res$	16	0.39
Upper Sheep (Big Sagebrush)		
$\log(K_\omega) = -1.28 - 2.48res - 6.3bascry$	24	0.76
$\log(K_{\omega(\mathrm{Max})}) = -0.92 - 2.31res - 7.03bascry$	24	0.68
Upper Sheep (Low Sagebrush)		
$\log(K_\omega) = -3.43$	12	
$\log(K_{\omega\ (\mathrm{Max})}) = -3.01$	12	
All Sites		
$\log(K_\omega) = -2.63 - 1.20res - 3.51bascry$	393	0.46
$\log(K_{\omega(\mathrm{Max})}) = -2.25 - 1.20res - 3.31bascry$	393	0.39

Table 10. Multiple Regressions Equations for Estimating the Average K_{τ_s} ($s\ m^{-1}$), and Maximum $K_{\tau_s(\mathrm{Max})}$ ($s\ m^{-1}$), Values of Flow Shear Stress Based Concentrated Flow Erodibility Coefficients as a Function of Basal Plant and Cryptogam Cover (*bascry*), Plant Litter (*res*), and Rock Cover (*rock*) for Each Site in This Study

Equation	n	R^2
Breaks		
$\log(K_{\tau_s}) = -2.98 - 1.78res + 8.38rock$	66	0.29
$\log(K_{\tau_s(\mathrm{Max})}) = -2.08 - 2.12res$	66	0.21
Castlehead		
$\log(K_{\tau_s}) = -3.76 + 1.75rock$	28	0.19
$\log(K_{\tau_s(\mathrm{Max})}) = -3.01 + 1.95rock$	28	0.18
Denio		
$\log(K_{\tau_s}) = -3.22 - 1.20res - 1.75bascry$	109	0.49
$\log(K_{\tau_s(\mathrm{Max})}) = -2.53 - 1.43res - 1.82bascry$	109	0.48
Marking Corral		
$\log(K_{\tau_s}) = -3.54$	58	
$\log(K_{\tau_s(\mathrm{Max})}) = -2.92$	58	
Onaqui		
$\log(K_{\tau_s}) = -3.61 + 0.53res$	80	0.18
$\log(K_{\tau_s(\mathrm{Max})}) = -3.10 + 0.55res$	80	0.11
Steens		
$\log(K_{\tau_s}) = -5.36$	16	
$\log(K_{\tau_s(\mathrm{Max})}) = -4.96$	16	
Upper Sheep (Big Sagebrush)		
$\log(K_{\tau_s}) = -2.05 - 1.66res - 5.81bascry$	24	0.54
$\log(K_{\tau_s(\mathrm{Max})}) = -2.25 - 9.85bascry$	24	0.40
Upper Sheep (Low Sagebrush)		
$\log(K_{\tau_s}) = -3.80$	12	
$\log(K_{\tau_s(\mathrm{Max})}) = -3.17$	12	
All Sites		
$\log(K_{\tau_s}) = -3.62 + 0.79rock - 1.74bascry$	393	0.18
$\log(K_{\tau_s(\mathrm{Max})}) = -3.04 + 0.88rock - 1.78bascry$	393	0.15

can be used as input parameters for concentrated flow erosion processes in physically based models. Erodibility and soil loss are generally low for undisturbed conditions, and therefore, within-storm erodibility decay is likely insignificant relative to total soil loss. Tree encroachment on the soil types studied, in contrast to burning, does not promote an instantaneously elevated sediment pulse of limited supply during runoff events. Rather, tree encroachment in sagebrush steppe enhances overall erodibility of shrub-interspaces and results in fairly consistent within-event sediment supply, detachment, and erodibility. Therefore, modeling within-event erodibility variation for undisturbed conditions or tree encroached sites likely will not improve overall model results. A multiple regression equation between the logarithm of erodibility at undisturbed sites and tree encroached sites as a dependent variable and litter cover (*res*), rock cover (*rock*), basal plant and cryptogam cover (*bascry*), and soil clay (*clay*) and silt (*silt*) amounts as independent variables resulted into the following equation:

$$\log(K_\omega) = -4.14 - 1.28res - 0.98rock - 15.16clay + 7.09silt \quad (n = 163,\ R^2 = 0.72), \tag{17}$$

where all independent variables are in decimal fraction. Reapplying the multiple regressions in equation (17) but with combining the vegetation cover (i.e., basal plant and residue) into one variable resulted into the following equation:

$$\log(K_\omega) = -4.05 - 0.81\,(res + bascry) - 11.87clay + 5.19silt \quad (n = 163,\ R^2 = 0.72). \tag{18}$$

Equations (17) and (18) can estimate average erodibility for a wide range of undisturbed rangeland sites and tree encroached sites. In addition, both equations address the decrease of erodibility of the tree encroached sites due to the ecological recovery process using the vegetation cover attributes. Combining the vegetation and residue cover in one variable may be beneficial when isolated data for basal plant and litter is not available.

[32] On recently burned sites where sediment availability increases suddenly, within-event erodibility variation will often be too great to ignore. Since the decay factor did not follow any general trend with time postdisturbance and had little variation, and as most of its variation cannot be explained by any measured variable, a single value (i.e., median) can be assigned for the purpose of modeling. The

median value of decay factor β in the burned sites was -5.53 m^{-2}. In order for a model to predict the correct total of sedimentation when using decay function, the adjusted maximum erodibility, which is the intercept of regression between K_ω and q_c (see Figure 1), can be used for parameterization. A multiple regression equation between the logarithm of adjusted maximum erodibility at all burned sites as a dependent variable and vegetation cover, rock cover, and soil texture indices as independent variables resulted into the following equations:

$$\log(K_{\omega(\max)\mathrm{adj}}) = -3.28 - 1.77res - 1.26rock - 2.46bascry + 3.53silt \quad (n = 171,\ R^2 = 0.47), \tag{19}$$

$$\log(K_{\omega(\max)\mathrm{adj}}) = -3.64 - 1.97(res + bascry) - 1.85rock - 4.99clay + 6.06silt \quad (n = 171,\ R^2 = 0.47), \tag{20}$$

where $K_{\omega(\max)\mathrm{adj}}$ is the maximum erodibility corresponding to the decay factor of -5.53 m^{-2}. Equations (19) and (20) can predict maximum erodibility for a wide range of burned rangeland sites including burned tree encroached sites. In addition, including vegetation cover in these equations addresses the decrease of maximum erodibility of the burned sites due to the ecological recovery process. Applying estimated $K_{\omega(\max)\mathrm{adj}}$ from equations (19) and (20) in equation (13) with a decay value of -5.53 m^{-2} can estimate the erodibility within a hillslope flow event.

[33] In the case where physically based models cannot be changed from steady state to dynamic erosion process, the following multiple regression equations can be used for estimating the average steady state erodibility for burned sites:

$$\log(K_\omega) = -3.22 - 2.08res - 1.75rock - 2.70bascry + 3.64silt \quad (n = 206,\ R^2 = 0.52), \tag{21}$$

$$\log(K_\omega) = -3.29 - 2.25(res + bascry) - 1.82rock + 3.95silt \quad (n = 206,\ R^2 = 0.52). \tag{22}$$

[34] In the case where further differentiation between burned and unburned sites is not available, then the following regression equations can be used for estimating the average steady state erodibility:

$$\log(K_\omega) = -3.48 - 2.0res - 1.73rock - 1.41bascry - 10.35clay + 6.01silt \quad (n = 369,\ R^2 = 0.59), \tag{23}$$

$$\log(K_\omega) = -3.37 - 1.85(res + bascry) - 1.52rock - 9.20clay + 5.28silt \quad (n = 369,\ R^2 = 0.59). \tag{24}$$

The equations that describe shear stress erodibility corresponding to the aforementioned equations are presented in Table 11.

[35] While each physically based model uses different hydraulic parameters as the indicator for erosion rate, using stream power based equations (17) through (24) have several advantages. First, the results indicate that stream power is the best predictor for soil erosion on sites with high disturbance. These sites are most important to model as they represent the highest risk for erosion. Second, linearity of stream power versus detachment capacity in this study makes the concentrated flow erosion component simpler and easier to couple with other components in a model. Third, these equations do not have critical values that reduce the parameters needed for the model. Fourth, the equations use readily available data for estimating erodibility values. It is important to mention here that we caution against using the aforementioned equations with data that fall outside the ranges of values from which the regression equations were developed. Ranges of values for each variable used in each equation development are given in Table 12.

Table 11. Multiple Regressions Equations for Estimating the Average K_{τ_s} (s m^{-1}), and Adjusted Maximum K_{τ_s} (s m^{-1}) Based on Decay Factor of -5.27 m^{-2}, Values of Flow Shear Stress Based Concentrated Flow Erodibility Coefficients for Undisturbed and Disturbed Sites, as a Function of Basal Plant and Cryptogam Cover (*bascry*), Plant Litter (*res*), Rock Cover (*rock*), Silt (*silt*), and Clay (*clay*)

Equation	Equation Number	n	R^2
Unburned Sites			
$\log(K_{\tau_s}) = -4.94 + 1.77bascry - 17.35clay + 6.78silt$	(25)	163	0.63
$\log(K_{\tau_s}) = -4.19 - 15.25clay + 4.73silt$	(26)	163	0.59
Burned Sites			
Dynamic erodibility (decay factor = −5.27)			
$\log(K_{\tau_s(\max)\mathrm{adj}}) = -3.91 - 1.23bascry + 2.31silt$	(27)	175	0.16
$\log(K_{\tau_s(\max)\mathrm{adj}}) = -4.41 - 4.20clay + 4.50silt$	(28)	175	0.13
Steady state erodibility mode			
$\log(K_{\tau_s}) = -3.69 - 1.87bascry + 4.11clay$	(29)	206	0.17
$\log(K_{\tau_s}) = -3.96 - 0.81(res + bascry) - 1.21rock + 2.71silt$	(30)	206	0.15
All Sites			
$\log(K_{\tau_s}) = -4.21 - 0.33res - 10.16clay + 4.28silt$	(31)	369	0.32
$\log(K_{\tau_s}) = -4.14 - 0.27(res + bascry) - 9.70clay + 3.98silt$	(32)	369	0.32

Table 12. Ranges of Variables Used to Develop Equations (17) Through (32)

Variable	Equations Numbers							
	(17) and (25)	(18) and (26)	(19) and (27)	(20) and (28)	(21) and (29)	(22) and (30)	(23) and (31)	(24) and (32)
res	0.01 to 0.95	–	0.01 to 0.87	–	0.01 to 0.87	–	0.01 to 0.95	–
rock	0 to 0.78	0 to 0.78	0 to 0.53	0 to 0.53	0 to 0.54	0 to 0.54	0 to 0.78	0 to 0.78
bascry	0 to 0.58	–	0 to 0.47	–	0 to 0.47	–	0 to 0.58	–
(res + bascry)	–	0.02 to 1	–	0.01 to 0.88	–	0.01 to 0.88	–	0.01 to 1
clay	0.03 to 0.18	0.03 to 0.18	0.03 to 0.18	0.03 to 0.18	0.03 to 0.18	0.03 to 0.18	0.03 to 0.18	0.03 to 0.18
silt	0.1 to 0.52	0.1 to 0.52	0.24 to 0.52	0.24 to 0.52	0.24 to 0.52	0.24 to 0.52	0.1 to 0.52	0.1 to 0.52

[36] Decay factors in Table 5 were developed from data with the assumption that cumulative unit flow discharge starts to add up when erodibility is equal to $K_{(\mathrm{Max})}$ (i.e., $q_c = 0$ at $K = K_{(\mathrm{Max})}$). Hence it is important to detect when this maximum value occurred. One method could be to use the time where overland flow has a greater chance to form concentrated flow, such as at the peak flow rate.

[37] Note that equation (8), which describes the sediment mass-continuity relationship currently used in RHEM, is not time dependent. In other words, RHEM currently uses a steady state solution to the sediment continuity equation. Therefore a significant modeling implication of this study is that in order to use the time dependent erodibility relationships found here (i.e., equation (13)) the erosion model solution used must include a time dependent term, and thus the sediment continuity equation must be formulated as a partial differential equation including the time derivative for sediment concentration or load.

5. Conclusions

[38] In this study, concentrated flow simulations on disturbed and undisturbed rangeland were used to estimate the erodibility as well as to evaluate the performance of linear and power law equations that describe the relationship between erosion rate and several hydraulic parameters. The results showed that, in general, stream power provided the best linear function to describe the detachment rate at disturbed rangeland sites. Flow shear stress also performed well in describing detachment rate except at low erosion sites. Unit length shear force, on the other hand, performed poorly. The power law function did not improve the detachment relation over that of the linear function in all the cases of hydraulic parameters.

[39] The results showed that, in general, concentrated flow erodibility increased significantly when a site was exposed to a disturbance such as fire or tree encroachment. Fire not only facilitated increased erosive energy of overland flow and its impact by removing obstacles, but it also changed the soil properties affecting erodibility. However, fire impacts can vary among sites depending on the inherent characteristics of the site as well as on fire severity. Tree encroachment also changes the soil properties associated with erodibility in the area between trees even though the rate and magnitude of the impact is less than that of fire. The variation of average erodibility values in undisturbed sites and tree encroached sites within the recovering years was described very well ($R^2 = 0.72$) by empirical functions of readily available vegetation, rock cover, and soil texture data.

[40] The results also showed that concentrated flow erodibility was not constant within each experimental run. In most cases, especially in burned sites, erodibility had a high value at the beginning and then started to decline, mainly due to reduction of sediment availability. We developed an empirical equation to predict the change of erodibility as a function of cumulative unit discharge. The coefficients of these equations are the maximum initial value $K_{(\mathrm{Max})}$ and the decay factor β, where $K_{(\mathrm{Max})}$ variation within the recovering years was described reasonably ($R^2 = 0.47$) by empirical functions. The decay factor did not follow any general trend and can be approximated as an average value. The empirical function can be used for parameterizing the concentrated flow erosion component of physically based models for burned rangeland.

Notation

α power exponent of power law function.
β decay factor of erodibility exponential decaying function based on unit flow discharge, m^{-2}.
Γ unit length shear force, kg s^{-2}.
γ specific weight of water, kg m^{-2} s^{-2}.
τ_s flow shear stress, kg s^{-2} m^{-1}.
ω stream power, kg s^{-3}.
Ω unit stream power, m s^{-1}.
A flow cross section area, m^2.
bare fraction of bare soil area to the total ground area.
bascry fraction of area covered by basal plant and cryptogam to the total ground area.
clay fraction of surface soil (average of 0–4 cm depth) represented by clay.
d flow depth, m.
D_{cf} concentrated flow soil detachment rate capacity, kg s^{-1} m^{-2}.
D_r soil detachment rate, kg s^{-1} m^{-2}.
f_s hydraulic friction due to the soil grains.
f_t total Darcy-Weisbach friction factor.
G sediment transport rate, kg s^{-1}.
G_e sediment transport rate at the exit of plot, kg s^{-1}.
HP hydraulic parameter used to predict D_{cf}.
HP_c threshold value where D_{cf} is insignificant before *HP* exceeds it.
K erodibility factor.
K_Γ unit length shear force erodibility factor, s m^{-2}.
K_{τ_s} shear stress erodibility factor, s m^{-1}.
$K_{\tau_s(\mathrm{max})\mathrm{adj}}$ maximum shear stress erodibility factor corresponding to the decay factor of -5.27 m^{-2}, s m^{-1}.
K_ω stream power erodibility factor, s^2 m^{-2}.

$K_{\omega(\max)adj}$ maximum stream power erodibility corresponding to the decay factor of -5.53 m^{-2}, s^2 m^{-2}.
K_Ω unit stream power erodibility factor, kg m^{-3}.
K_{HP} soil erodibility factor based on the hydraulic parameter *HP*.
K_q unit discharge erodibility factor, kg m^{-4}.
$K_{(\max)}$ maximum measured erodibility within a flow release rate experimental run.
q unit discharge, m^2 s^{-1}.
Q flow discharge, m^3 s^{-1}.
q_c cumulative unit flow discharge, m^2.
res fraction of area covered by plant litter to the total ground area.
R_h flow hydraulic radius, m.
rock fraction of area covered by rock to the total ground area.
S average slope of the plot, m m^{-1}.
silt fraction of surface soil (average of 0–4 cm depth) represented by silt.
T_c sediment transport capacity, kg s^{-1}.
V flow velocity, m s^{-1}.
w flow width, m.

[41] **Acknowledgments.** The authors wish to thank the Natural Resources Conservation Service for funding of this project as part of the Grazing Lands component of the Conservation Effects Assessment Project (CEAP). The authors also wish to express appreciation to the Joint Fire Science Program for funding the field work associated with this project. Portions of the field research were funded by Joint Fire Science Program grants for investigating fire effects on rangeland runoff and erosion processes. Field studies at pinyon and juniper woodland sites in this project are part of the Sagebrush Treatment Evaluation Project (SageSTEP) funded by the U. S. Joint Fire Science Program. This is contribution 60 of the SageSTEP project. USDA is an equal opportunity provider and employer.

References

Al-Hamdan, O. Z., F. B. Pierson, M. A. Nearing, J. J. Stone, C. J. Williams, P. R. Kormos, J. Boll, and M. A. Weltz (2011), Shear stress partitioning of overland flow on disturbed and undisturbed rangelands, Paper 11134, paper presented at International Proceedings of the Symposium on Erosion and Landscape Evolution, September 18–21, 2011, Anchorage, Alaska, USA, American Society of Agricultural and Biological Engineers and Association of Environmental and Engineering Geologist.

Al-Hamdan, O. Z., F. B. Pierson, M. A. Nearing, J. J. Stone, C. J. Williams, C. A. Moffet, P. R. Kormos, J. Boll, and M. A. Weltz (2012), Characteristics of concentrated flow hydraulics for rangeland ecosystems: Implications for hydrologic modeling, *Earth Surf. Processes Landforms*, *37*, 157–168.

Allison, P. D. (1999), *Multiple Regression: A Primer*, Pine Forge Press, Oaks, CA.

Belnap, J., J. R. Welter, N. B. Grimm, N. Barger, and J. A. Ludwig (2005), Linkages between microbial and hydrologic processes in arid and semiarid watersheds, *Ecology*, *86*(2), 298–307.

Blackburn, H., Wilbert, F. B. Pierson, and M. S. Seyfried (1990), Spatial and temporal influence of soil frost on infiltration and erosion of sagebrush rangelands, *Water Resour. Bull.*, *26*(6), 991–997.

Cochrane, T. A., and D. C. Flanagan (1997), Detachment in a simulated rill, *Trans. ASAE*, *40*(1), 111–119.

De Baets, S., and J. Poesen (2010), Empirical models for predicting the erosion-reducing effect of plant roots during concentrated flow, *Geomorphology*, *118*, 425–432.

De Baets, S., J. Poesen, G. Gyssels, and A. Knapen (2006), Effects of grass roots on erodibility of topsoils during concentrated flow, *Geomorphology*, *76*, 54–67.

DeBano, L. F. (1991), The effect of fire on soil properties, in Proceedings—Management and Productivity of Western-Montane Forest Soils, edited by A. E. Harvey and L. F. Neuenschwander, pp. 151–156, *USDA Forest Service, General Technical Report, INT-280*, USDA Forest Serv., Ogden, Ut.

DeBano, L. F., D. G. Neary, and P. F. Ffolliott (1998), *Fire's Effects on Ecosystems*, John Wiley, New York.

Elliot, W. J., and J. M. Laflen (1993), A process-based rill erosion model, *Trans. ASAE*, *36*(1), 35–72.

Elliot, W. J., A. M. Liebenow, J. M. Laflen, and K. D. Kohl (1989), A compendium of soil erodibility data from WEPP cropland soil field erodibility experiments 1987–1988. *NSERL Rpt. No. 3*. Ohio State University and Natural Soil Erosion Research Laboratory, Agricultural Research Service, U.S. Department of Agriculture, W. Lafayette, Indiana.

Flanagan, D. C., and M. A. Nearing, Eds. (1995), USDA-Water Erosion Prediction Project (WEPP) hillslope profile and watershed model documentation, *NSERL Report No. 10*, National Soil Erosion Research Laboratory, USDA-Agricultural Research Service, West Lafayette, Indiana.

Flerchinger, G. N., and K. R. Cooley (2000), A ten-year water balance of a mountainous semi-arid watershed, *J. Hydrol.*, *237*, 86–99.

Foltz, R. B., H. Rhee, and W. J. Elliot (2008), Modeling changes in rill erodibility and critical shear stress on native surface roads, *Hydrol. Processes*, *22*, 4782–4788.

Foster, G. R. (1982), Modeling the erosion process, hydrologic modeling of small watersheds, in *American Society of Agricultural Engineers Monograph No. 5*, edited by, C. T. Haan, H. P. Johnson, and D. L. Brakensiek, pp. 297–380, American Society of Agricultural Engineers, St. Joseph, Michigan.

Franti, T. G., J. M. Laflen, and D. A. Watson (1999), Predicting soil detachment from high-discharge concentrated flow, *Trans. ASAE*, *42*(2), 329–335.

Giménez, R., and G. Govers (2002), Flow detachment by concentrated flow on smooth and irregular beds, *Soil Sci. Soc. Am. J.*, *66*, 1475–1483.

Giovannini, G., S. Lucchesi, and M. Giachetti (1988), Effect of heating on some physical and chemical parameters related to soil aggregation and erodibility, *Soil Sci.*, *146*, 255–261.

Govers, G. (1992), Relationship between discharge, velocity and flow area for rills eroding loose, non-layered materials, *Earth Surf. Processes Landforms*, *17*, 515–528.

Gyssels, G., J. Poesen, E. Bochet, and Y. Li (2005), Impact of plant roots on the resistance of soils to erosion by water: A review, *Prog. Phys. Geogr.*, *2*, 189–217.

Hairsine, P. B., and C. W. Rose (1992), Modeling water erosion due to overland flow using physical principles, 2. Rill Flow, *Water Resour. Res.*, *28*, 245–250.

Knapen, A., and J. Poesen (2010), Soil erosion resistance effects on rill and gully initiation points and dimensions, *Earth Surf. Processes Landforms*, *35*, 217–228.

Knapen, A., J. Poesen, G. Govers, G. Gyssels, and J. Nachtergaele (2007a), Resistance of soils to concentrated flow erosion: A review, *Earth Sci. Rev.*, *80*, 75–109.

Knapen, A., J. Poesen, P. Galindo-Morales, S. De Baets, and A. Pals (2007b), Effects of microbiotic crusts under cropland in temperate environments on soil erodibility during concentrated flow, *Earth Surf. Processes Landforms*, *32*, 1884–1901.

Knapen, A., J. Poesen, G. Govers, and S. De Baets (2008), The effects of conservation tillage on runoff erosivity and soil erodibility during concentrated flow, *Hydrol. Processes*, *2*(2), 1497–1508.

Laflen, J. M., W. J. Elliot, J. R. Simanton, C. S. Holzey, and K. D. Kohl (1991), WEPP Soil erodibility experiments for rangeland and cropland soils, *J. Soil Water Conserv.*, *46*(1), 39–44.

Line, D. E., and L. D. Meyer (1989), Evaluating interrill and rill erodibilities for soils of different textures, *Trans. ASAE*, *32*(6), 1995–1999.

Ludwig, J. A., B. P. Wilcox, D. D. Breshears, D. J. Tongway, and A. C. Imeson (2005), Vegetation patches and runoff-erosion as interacting ecohydrological processes in semiarid landscapes *Ecology*, *86*(2), 288–297.

McIver, J. D., et al. (2010), The Sagebrush Steppe Treatment Evaluation Project (SageSTEP): A test of state-and-transition theory, *Gen. Tech. Rep. RMRS-GTR-237*, US Department of Agriculture, Forest Service, Ft. Collins, CO, USA.

Megahan, W. F. (1974), Erosion over time: A model, *USDA–Forest Service Research Paper Report INT-156*. Intermountain Research Station: Ogden UT, 14 pp.

Miller, R. F., T. J. Svejcar, and J. R. Rose (2000), Impacts of western juniper on plant community composition and structure, *J. Range Manage.*, *53*, 574–585.

Miller, R. F., J. D. Bates, T. J. Svejcar, F. B. Pierson, and L. E. Eddleman (2005), Biology, ecology, and management of western juniper (Juniperus occidentalis), in *Technical Bull.* 152, 82 pp., Oregon State University, Agricultural Experiment Station, Corvallis, OR, USA.

Moffet, C. A., F. B. Pierson, P. R. Robichaud, K. E. Spaeth, and S. P. Hardegree (2007), Modeling soil erosion on steep sagebrush rangeland before and after prescribed fire, *Catena*, *71*(2), 218–228, doi:10.1016/j.catena.2007.03.008.

Moore, I. D., and G. J. Burch (1986), Modeling erosion and deposition: topographic effects, *Trans. ASAE*, *29*(6), 1624–1640.

Morgan, R. P. C., J. N. Quinton, R. E. Smith, G. Govers, J. W. A. Poesen, K. Auerswald, G. Chisci, D. Torri, and M. E. Styczen (1998), The European soil erosion model (EUROSEM): A dynamic approach for predicting sediment transport from fields and small catchments, *Earth Surf. Processes Landforms*, *23*, 527–544.

Nearing, M. A., G. R. Foster, L. J. Lane, and S. C. Finkner (1989), A processed based soil erosion model for USDA-water erosion prediction project technology, *Trans. ASAE*, *32*(5), 1587–1593.

Nearing, M. A., L. D. Norton, D. A. Bulgakov, G. A. Larionov, L. T. West, and K. M. Dontsov (1997), Hydraulics and erosion in eroding rills, *Water Resour. Res.*, *33*, 865–876.

Nearing, M. A., J. R. Simanton, L. D. Norton, S. Y. Bulygin, and J. Stone (1999), Soil erosion by surface water flow on a stony, semiarid hillslope, *Earth Surf. Processes Landform*, *24*, 677–686.

Nearing, M. A., H. Wei, J. J. Stone, F. B. Pierson, K. E. Spaeth, M. A. Weltz, D. C. Flanagan, and M. Hernandez (2011), A rangeland hydrology and erosion model, *Trans. Am. Soc. Agric. Bio. Eng.*, *54*, 901–908.

Pierson, F. B., P. R. Robichaud, and K. E. Spaeth (2001), Spatial and temporal effects of wildfire on the hydrology of a steep rangeland watershed, *Hydrol. Processes*, *15*, 2905–2916.

Pierson, F. B., D. H. Carlson, and K. E. Spaeth (2002), Impact of wildfire on soil hydrological properties of steep sagebrush-steppe rangeland, *Intl. J. Wildland Fire*, *11*, 145–151.

Pierson, F. B., J. D. Bates, T. J. Svejcar, and S. P. Hardegree (2007), Runoff and erosion after cutting western juniper, *Rang. Ecology Manage.*, *60*, 285–292.

Pierson, F. B., P. R. Robichaud, C. A. Moffet, K. E. Spaeth, S. P. Hardegree, P. E. Clark, and C. J. Williams (2008), Fire effects on rangeland hydrology and erosion in a steep sagebrush-dominated landscape, *Hydrol. Processes*, *22*, 2916–2929, doi:10.1002/hyp.6904.

Pierson, F. B., C. A. Moffet, C. J. Williams, S. P. Hardegree, and P. Clark (2009), Prescribed-fire effects on rill and interrill runoff and erosion in a mountainous sagebrush landscape, *Earth Surf. Processes Landforms*, *34*, 193–203.

Pierson, F. B., C. J. Williams, P. R. Kormos, S. P. Hardegree, and P. E. Clark (2010), Hydrologic vulnerability of sagebrush steppe following pinyon and juniper encroachment, *Rang. Ecol. Manage.*, *63*, 614–629, doi:10.2111/REM-D-09-00148.1.

SAS Institute Inc. (2007), *SAS for Windows*, SAS Institute Inc., Cary, NC.

Simanton, J. R., M. A. Weltz, and H. D. Larsen (1991), Rangeland experiments to parameterize the water erosion prediction project model: Vegetation canopy cover effects, *J. Range Manage.*, *44*(3), 276–282.

Snyman, H. A. (2003), Short-term response of rangland following an unplanned fire in terms of soil characteristics in semi-arid climate of South Africa, *J. Arid Environ.*, *55*, 160–180.

Ubeda, X., and L. R. Outeiro (2009), Physical and chemical effects of fire on soil, in *Fire Effects on Soils and Restoration Strategies*, Vol. 5, edited by Cerda, A. and P. R. Robichaud, 605 pp., Land Reconstruction and Management Series, Science Publishers, Enfield, NH.

Wagenbrenner, J. W., P. R. Robichaud, and W. J. Elliot (2010), Rill erosion in natural and disturbed forests: 2. Modeling Approaches, *Water Resour. Res.*, *46*, W10507, doi:10.1029/2009WR008315.

Wei, H., M. A. Nearing, J. J. Stone, D. P. Guertin, K. E. Spaeth, F. B. Pierson, M. H. Nichols, and C. A. Moffett (2009), A new splash and sheet erosion equation for rangelands, *Soil Sci. Soc. Am. J.*, *73*(4), 1386–1392.

Zhang, G., B. Liu, G. Liu, X. He, and M. A. Nearing (2003), Detachment of undisturbed soil by shallow flow, *Soil Sci. Soc. Am. J.*, *67*, 713–719.

Zhu, J. C., C. J. Gantzer, S. H. Anderson, R. L. Peyton, and E. E. Alberts (2001), Comparison of concentrated flow-detachment equations for low shear stress, *Soil Tillage Res.*, *61*, 203–212.

Ziegler, A. D., T. W. Giambelluca, and R. A. Sutherland (2002), Improved method for modeling sediment transport on unpaved roads using KINEROS2 and dynamic erodibility, *Hydrol. Processes*, *16*, 3079–3089.